Title: Single-cell profiling of multiple myeloma reveals molecular response to FGFR3 inhibitor despite clinical progression

Running Title: Single-cell analysis of targeted therapy response

Authors: Danielle C. Croucher[1,2], Anup Joseph Devasia[1], Dor D. Abelman[1,2], Ali Mahdipour-Shirayeh[1], Zhihua Li[1], Natalie Erdmann[1], Rodger Tiedemann[1,2], Trevor J. Pugh[1,2,5,*], Suzanne Trudel[1,2,*]

Affiliations:

[1]Princess Margaret Cancer Centre, University Health Network, Toronto, Ontario, Canada.

[2]Department of Medical Biophysics, University of Toronto, Toronto, ON, Canada.

[3]Department of Medicine, McGill University, Montréal, QC, Canada.

[4]Division of Hematology/Oncology, Mayo Clinic, Scottsdale, AZ, USA

[5]Ontario Institute for Cancer Research, Toronto, ON, Canada.

[*]Correspondence to:

E-mail: trevor.pugh@utoronto.ca (T.J.P); Suzanne.Trudel@uhn.ca (S.T.)

Phone: 416-581-7689 (T.J.P); 416-946-4587 (S.T.)

The authors declare no potential conflicts of interest.

ABSTRACT

Genomic characterization of cancer has enabled identification of numerous molecular targets, which has led to significant advances in personalized medicine. However, with few exceptions, precision medicine approaches in the plasma cell malignancy multiple myeloma (MM) have had limited success, likely owing to the subclonal nature of molecular targets in this disease. Targeted therapies against FGFR3 have been under development for the past decade in the hopes of targeting aberrant FGFR3 activity in MM. FGFR3 activation results from the recurrent transforming event of t(4;14) found in approximately 15% of MM patients, as well as secondary FGFR3 mutations in this subgroup. To evaluate the effectiveness of targeting FGFR3 in MM, we undertook a phase 2 clinical trial evaluating the small molecule FGFR1-4 inhibitor, erdafitinib, in relapsed/refractory myeloma patients with or without FGFR3 mutations (NCT02952573). Herein, we report on a single t(4;14) patient enrolled on this study who was identified to have a subclonal *FGFR3* stop-loss deletion. Although this individual eventually progressed on study and succumbed to their disease, the intended molecular response was revealed through an extensive molecular characterization of the patient's tumour at baseline and on treatment using single-cell genomics. We identified elimination of the *FGFR3*-mutant subclone after treatment and expansion of a pre-existing clone with loss of chromosome 17p. Altogether, our study highlights the utility of single cell genomics in targeted trials as they can reveal molecular mechanisms that underlie sensitivity and resistance. This in turn can guide more personalized and targeted therapeutic approaches, including those that involve FGFR3-targeting therapies.

INTRODUCTION

The treatment landscape for multiple myeloma (MM) has changed dramatically over the past 2 decades. Immune-based therapies have become the standard of care for this hematological malignancy, especially at relapse. Advances in molecular profiling and sequencing have enabled a better understanding of the molecular drivers underlying the initiation and progression that underlie myeloma pathogenesis. The main initiating events are hyperdiploidy and immunoglobulin heavy chain (IgH) translocations with one of five recurrent partner loci: *CCND1* in t(11;14), *MMSET/FGFR3* in t(4;14), *MAF* in t(14;16), *MAFB* in t(14;20), and *CCND3* in t(6;14). Subsequent progression of the disease is marked by the acquisition of additional somatic mutations, indels, and copy number alterations, which underlies drives evolution and therapeutic resistance (Pawlyn and Davies 2018).

The t(4;14) translocation is found in approximately 15% of MM patients and is believed to be a high-risk molecular marker with adverse survival rates (Abdallah et al. 2020). The translocation results in ectopic and overexpression of *FGFR3* in nearly 80% of newly diagnosed t(4;14) patients, with the remainder lacking expression due to the loss of the der(14) chromosome (Benard et al. 2017). The lack of *FGFR3* expression in a subset of t(4;14) MM has raised questions regarding its relevance in oncogenic transformation. Meanwhile, whole exome sequencing (WES) of 80 t(4;14) cases from the MMRF CoMMpass study (NCT01454297) identified non-synonymous mutations of *FGFR3* in 20% of patients and posit that these mutations are likely to occur after the primary translocation event (Benard et al. 2017). Common *FGFR3* mutations in t(4;14) patients occur in the extracellular (p.R248), transmembrane (p.Y373), kinase domains (p.K650), and stop codon (p.J807G, p.J807R and p.J807C) resulting in augmented receptor dimerization and ligand-independent signalling and have been shown to be strongly transforming in several experimental models (Wesche et al. 2011; Plowright et al. 2000; Chesi et al. 2001). Supporting the clinical relevance of *FGFR3* mutations in myeloma patients with t(4;14), *FGFR3*^{mut} expressing patients had a median survival of 2.8 years compared to not reached for t(4;14) *FGFR3*^{wt} expressing patients (Benard et al. 2017). Given the various ways that *FGFR3* can be dysregulated in MM and the associated adverse prognosis conferred to this patient population, new treatments tailored to this molecular subgroup are needed, as is a more in-depth understanding of the molecular dynamics of treatment response.

Based on pre-clinical studies demonstrating anti-myeloma activity of FGFR3 inhibition in t(4;14) myeloma (Trudel et al. 2004), we initiated a phase 2 clinical trial to evaluate the efficacy of erdafitinib, a potent tyrosine kinase inhibitor of FGFR1-4, plus dexamethasone in t(4;14) relapsed or refractory myeloma (NCT02952573). Participants in the study were assigned to one of two groups depending on whether they expressed wild-type *FGFR3* or harbored a somatic mutation of *FGFR3* (Supplementary Figure 1). We report the changes in genomic landscape pre- and post-treatment in a t(4;14) $FGFR3^{mut}$ myeloma patient who was enrolled in this clinical trial.

RESULTS

Clinical presentation and molecular profiling

A 52 year old female was diagnosed with IgA lambda MM, t(4;14) positive, ISS-III in February 2014 (Supplementary Figure 1A). Her initial treatment included triplet induction (cyclophosphamide-bortezomib-dexamethasone) followed by autologous stem cell transplantation (ASCT) and 4 cycles of lenalidomide/dexamethasone consolidation followed by lenalidomide maintenance. She experienced disease progression within one year of ASCT and subsequently received multiple lines of therapy including carfilzomib based (carfilzomib-lenalidomide-dexamethasone), selinexor based (selinexor-pomalidomide-dexamethasone), and daratumamab based (daratumamab-pomalidomide-dexamethasone) regimens, as well as intensive therapy with DPACE (dexamethasone-cisplatin-adriamycin-cyclophosphamide-etoposide). Following DPACE chemotherapy, she experienced prolonged bone marrow suppression, eventually demonstrating biochemical progression upon count recovery. Clinical molecular profiling performed prior to subsequent treatment (Supplementary Figure 1A), confirmed high expression of *FGFR3*, the presence of *IGHA1-FGFR3* fusion transcripts indicative of t(4;14), and an activating stop-loss, in-frame 30 bp deletion in *FGFR3* (c.2404_*12delGGGGGCTCGCGGACGTGAAGGGCCACTGGT, p.G802_X807del). The patient was therefore enrolled onto a phase 2 clinical trial evaluating the oral, small molecule FGFR3 inhibitor, erdafitinib in patients expressing *FGFR3* with or without mutation (NCT02952573, Supplementary Figure 1B). Two months into treatment with erdafitinib, the patient demonstrated evidence of biochemical progression (Supplementary Table 1), eventually succumbing to the disease one month later.

Clinical tumour sequencing for this patient was performed as part of the Multiple Myeloma Research Foundation's (MMRF) Michigan Oncology Sequencing Center (MI-ONCOSEQ) clinical sequencing study (NCT0288410) using the OncoSeq 1500 assay (CLIA-certified laboratory-developed test), which targets 1500 cancer-related genes (4.6 Mb). Briefly, a bone marrow (BM) aspirate and peripheral blood sample were collected from the patient and shipped overnight to the Michigan Centre for Translational Pathology (Supplementary Figure 1A). Tumour (CD138+ enriched cells) and normal (CD138-depleted peripheral blood mononuclear

cells) target capture libraries and tumour whole transcriptome capture libraries were prepared and sequenced according to the study protocol on a HiSeq2500 (500x coverage for each tumour sample, 200x coverage for matched normal, and 40 million paired end reads for tumour transcriptome sequencing). Sequencing QC reported an estimated 46% tumour content after sequencing and passing scores for nucleic acid quality, sequencing quality, library quality, and SNP fingerprinting. In the cancer cells, the OncoSeq assay detected a gain of chromosome 1, loss of chromosomes 13 and X, a somatic subclonal in-frame stop-loss mutation in *FGFR3* (p.G802_X807del, AF=20%), and 4 non-synonymous, subclonal somatic mutations of unknown significance: *EED* (p.H258N, AF=10%), *LRP1B* (p.T1099A, AF=15%), *MYC* (p.A416S, AF=20%), and *BCOR* (p.A184V, AF=19%) (Table 1, Supplementary Table 2). Although the assay does not directly detect IgH translocations, the sample had evidence of the t(4;14) rearrangement at *FGFR3*/*WHSC1* as supported by gene fusion transcripts with *IGHA1* and outlier expression of *FGFR3* from RNA-seq analysis.

Single-cell Expression Analysis

To understand the molecular underpinnings of the response to erdafitinib treatment, BM samples were collected prior to erdafitinib treatment initiation (pre-treatment) and after 28 days of erdafitinib treatment at cycle 2 day 1 (C2D1). Mononuclear cells isolated from the BM were then profiled using the 10x Genomics single-cell RNA-sequencing platform. This resulted in high-quality single-cell expression profiles for 1,130 and 910 cells, respectively for pre-treatment and C2D1 samples (Supplementary Table 3). Myeloma cell clusters (C1, C2, C5, C7, n= 905 cells) were subset bioinformatically from the full BM mononuclear cell dataset (Supplementary Figure 2A) based on cluster enrichment for expression of myeloma cell markers *SDC1* (CD138), *TNFRSF17* (BCMA), and *FGFR3* (Supplementary Figure 2B). This subset of myeloma cells were then re-clustered to reveal transcriptional heterogeneity within the malignant cell compartment, with 4 unique clusters (Fig. 1A). From the pre-treatment sample, myeloma cells predominantly clustered into 2 populations: C1 and C2 (Fig. 1A-C). As shown in Figure 1D, C1 was characterized by the expression of genes associated with plasma cell differentiation, the endoplasmic reticulum, and protein processing (*JCHAIN, SSR4, XBP1, CD48*), while C2

upregulated expression of the *FGFR3* target gene *CCL3* (Masih-Khan et al. 2006). Cells from the C2D1 sample also co-localized in C1, as well as in two other predominant clusters, C0 and C3 (Fig. 1A-C), which expressed genes related to programmed cell death prevention (*BCL2, PIM2, TRADD, BEX2*) and cell cycle/proliferation (*MKI67, TOP2A, BIRC5*), respectively (Fig. 1D). This supports the presence of transcriptional variability in the malignant cell compartment, and a shift in expression profiles upon treatment that may reflect cellular programs of resistance to erdafitinib.

We next evaluated how the observed transcriptional heterogeneity relates to the copy number variations (CNVs) reported by the clinical sequencing conducted for this patient. To do this, we inferred CNVs in each myeloma cell using the sciCNV method with 60 normal plasma cells from 2 donors from published datasets as a reference (Zheng et al. 2017). As seen in Figure 2A and consistent with clinical tumour sequencing results (Supplementary Table 2), sciCNV accurately detected the gain of chromosome 1q and loss of chromosome 13 in both the pre-treatment and C2D1 samples. However, we did not detect deletion of chromosome X, which we suspect may be attributed to sex differences between the patient and that of the subjects used for normal plasma cell references, since one of the donors is male based on chrY gene expression (Supplementary Figure 3A).

In addition to the clinical results from bulk DNA sequencing, sciCNV also detected a focal gain of chromosome 22 in both samples, a gain of chromosome 4 in the pre-treatment sample and the loss of chromosome 17p in the C2D1 sample. We in turn used shallow whole genome sequencing (WGS) of CD138-selected cells from the pre-treatment sample, which validated the presence of a gain of chromosome 4 (Supplementary Figure 3B). However, this validation method did not detect the gain in chromosome 22 which we hypothesize may be an artifact from scRNA-seq expression-based CNV inference related to high expression of immunoglobulin light chain genes which are localized in this genomic region (Supplementary Figure 3C).

Given that deletion of chromosome 17p is a known poor prognostic event in myeloma, we hypothesized that erdafitinib treatment led to expansion of an aggressive del17p subclone. As predicted, we identified 3 cells from the pre-treatment sample that scored lower for a chromosome 17p gene set (Fig. 2B, less than 25th percentile of chromosome 17p score in C2D1

cells) suggesting that a rare subpopulation of cells pre-existing before treatment contained deletion of chromosome 17p, which then expanded upon treatment with erdafitinib. To validate this hypothesis, we profiled pre-treatment and C2D1 cells using fluorescence in situ hybridization (FISH) with probes for chromosomes 1, 4, 13, 14, and 17. Consistent with our scRNA-seq data, del17p was detected in t(4;14) positive cell populations at a frequency of 0.63% pre-treatment and 84.6% at C2D1 (Fig. 2C-D). Thus, our data confirms that a chromosome 17p deletion subclone pre-existed and expanded rapidly during erdafitinib therapy (Fig. 2C-D).

In addition to copy number variants, the clinical panel sequencing of this tumour revealed the presence of a subclonal FGFR3 in-frame stop-loss mutation (p.G802_X807del) which is predicted to result in protein elongation as the last five amino acids are replaced by aberrant amino acids. Since this deletion occurs in the 3-prime end of the *FGFR3* gene, which is enriched in scRNA-sequencing, we evaluated whether the p.G802_X807del stop-loss aberration could be detected in myeloma cells from our scRNA-seq data. Indeed, we identified 5 reads with coverage of the mutation site, which corresponded to 4 cells (3 cells with 1 mutant read and 1 cell with 2 mutant reads, Fig. 3A). We then mapped the cell barcodes back to our clustering results and found that all 4 cells with the FGFR3 stop-loss mutation were located in the pre-treatment sample, cluster C2 (Fig. 3B). Notably, our single-cell analysis of transcriptional heterogeneity revealed *FGFR3* target genes such as *CCL3* were particularly upregulated in C2 relative to all other clusters suggesting that *FGFR3* p.G802_X807del may confer enhanced or ligand-independent activity to the FGFR3 receptor tyrosine kinase. Since 90.8% of the C2 cluster is comprised of cells from the pre-treatment sample (109/120 cells) compared to 9.2% cells (11/120 cells), from the sample taken after 28 days of erdafitinib treatment, we suspect that cells containing this aberration may be particularly sensitive to erdafitinib. Thus, although this patient did not display a reduction of M protein and free light chains as conventional markers of disease response, molecular profiling revealed a marked reduction in the small cell cluster containing the *FGFR3* mutation and *CCL3* upregulation indicative of a molecular response to erdafitinib (Fig. 3C).

DISCUSSION

Characterization of human cancers using genomic technologies has allowed the identification of numerous molecular targets, which has led to significant advances in drug development and personalized medicine. However, with few exceptions (e.g. venetoclax in t(11;14) MM patients (Kaufman et al. 2021)), precision medicine approaches for MM have had limited success, likely owing to the subclonal nature of molecular targets. Our study demonstrates that the use of scRNA-seq to profile the molecular landscape of tumors extracted pre- and post- treatment with targeted agents can reveal significant insights into the underlying genomic and transcriptomic features of response and resistance. Our analysis of the patient's tumour at multiple timepoints revealed multiple subclonal malignant populations and rapid selection of a rare, resistant subclone indicating the necessity for combinatorial treatment approaches in patients with subclonal *FGFR3* mutations. In our study, this resistant subclone demonstrated acquired deletion of chromosome 17p, which is associated with reduced overall survival in patients with MM (Lakshman et al. 2019). Notably, bulk clinical sequencing prior to trial enrolment did not identify the subclonal deletion of chromosome 17p in this patient, likely because of limits of detection given the low allele frequency of this variant (as confirmed by FISH). Thus, our data provide rationale for the use of single-cell profiling in patients receiving targeted therapy, as it may permit the identification of subclones likely to escape the activity of certain targeted therapies. Indeed, our study and the use of single-cell RNA-seq provides insight into mechanisms of drug resistance suggesting that *TP53* deletion via loss of 17p may confer FGFR3 inhibitor resistance, consistent with similar reports for EGFR inhibitors in lung cancer (Huang et al. 2011). The integration of single-cell genomics into precision medicine trials may allow for implementation of more personalized and rational combinatorial approaches that target the various subclones of a given myeloma tumour. Indeed, investigating combination therapies using a genomics-driven approach for molecularly-targeted therapy matching is currently being taken by the MMRF MyDrug study (NCT03732703) (Kumar et al. 2022).

Our use of single-cell RNA-sequencing indirectly permitted multi-modal profiling of genetic alterations in individual myeloma cells and linkage of an *FGFR3* sequence mutation to disruption of gene expression programs in a subclonal population. More specifically, we identified the *FGFR3* p.G802_X807del aberration in the scRNA-sequencing reads of our data

and showed that these cells clustered in the same transcriptional subgroup (C2). While this specific aberration has not yet been described in the literature, several missense stop-loss mutations in the stop codon loci have been reported (p.X807G, p.X807R, and p.X807C) and result in the same read-through of the stop codon (Rousseau et al. 1995). Several activating FGFR3 mutations have been described in myeloma (Onwuazor et al. 2003; Ronchetti et al. 2001; Chesi et al. 2001) and render FGFR3 ligand-independent through changes in the intracellular domain activation loop (p.K650E), or in the extracellular domain (p.Y373C). Functional analysis of various FGFR3 mutants in the context of bone growth disorders has been reported including those in the intracellular domain (p.K650E, p.X807R), the transmembrane domain, and the extracellular domain (p.Y373C), which revealed that receptor phosphorylation is greater for FGFR3 mutations in the intracellular domain, which includes p.X807R, and that p.X807R results in a constitutively active FGFR3 (Gibbs and Legeai-Mallet 2007). While a functional analysis of the downstream effects of p.G802_X807del is beyond the scope of this report, our scRNA-seq data support indirectly that this aberration would have similar downstream effects to p.X807R, since cells expressing the *FGFR3* stop-loss allele in our study demonstrated upregulation of FGFR3-target genes *CCL3* and *CCL4* (Masih-Khan et al. 2006) beyond that seen in cells with the t(4;14) translocation alone. Further, it is intriguing that the cells predicted to lack the mutation harbored an expression profile of increased differentiation and endoplasmic reticulum/protein processing since our previous work has demonstrated functional maturation of myeloma cells when mutated FGFR3 is inhibited (Trudel et al. 2004). This would further support the constitutive activation of FGFR3 in cluster C2 preventing the completion of normal differentiation programs and onset of high-level antibody secretion, as we have previously shown.

Our data revealed that the C2 malignant subpopulation, which contained p.G802_X807del-expressing cells, was almost completely eliminated by treatment with erdafitinib. However, given that t(4;14) is an initiating event in myeloma and thus presumably all cells expressed this translocation, including the erdafitinib-resistant subclone, our data supports that targeting wild-type FGFR3 on a t(4;14) background may not be effective. Rather, our data suggest that the mechanism of action for erdafitinib is targeted towards aberrant FGFR3 activity via FGFR3 mutation. Thus, although this patient succumbed to clinical disease progression, a dramatic

molecular response was achieved with erdafitinib as evidenced by elimination of the intended *FGFR3*-mutant subclone. This is particularly important in light of several FGFR3-targeted clinical trials in MM showing best responses of stable disease, leading some to question whether this class of agents has a role in myeloma therapy (Arnulf et al. 2007; Scheid et al. 2015; Trudel et al. 2012). However, our study shows that measuring molecular responses at the single-cell level may more accurately reflect the effectiveness of targeted agents such as erdafitinib. Further, the incorporation of scRNA-seq companion studies is critically important for informing whether these agents are indeed effective against their intended target, and present an opportunity to dissect responses to combination therapies directed against different subclonal populations. Taken together, our findings support the continued exploration FGFR3-targeted agents in the t(4;14) subtype of myeloma that express FGFR3 mutations and highlight some key molecular insights provided by clinical single-cell profiling approaches in cancer therapeutics.

METHODS

Bone Marrow Collection and Processing

Bone marrow aspirates were obtained with consent under the study protocol approved by the Research Ethics Board at University Health Network, Toronto, Canada (CAPCR #16-5997). Samples were collected using fine-needle aspiration of the iliac crest into EDTA tubes and immediately transferred to the research laboratory for processing. Samples were diluted with PBS, and the mononuclear cell fraction was enriched for using density-based cell separation (Ficoll-Paque PLUS, GE Healthcare). Residual contaminating red blood cells were subsequently removed using ACK lysis buffer. After washing in PBS, cells were examined for quantity and viability using trypan blue and a Countess II automated counter (Thermo Fisher Scientific, Burlington, ON, Canada). Cells were then loaded into the 10x Genomics Chromium device according to the manufacturer's instructions.

Single-Cell Sequencing using 10x Genomics Chromium Device

Single-cell libraries were constructed using the 3' V2 chemistry kit from 10x Genomics (Plesanton, CA, US) according to manufacturer's instructions. Libraries were sequenced on an Illumina HiSeq 2500 targeting 60,000 reads/cell. The 10x Genomics CellRanger software suite (v2.0.1) was used for processing raw sequencing reads, alignment (GRCh38) and to generate a digital gene expression (DGE) matrix of genes-by-cell UMI counts. Sequencing metrics can be found in Supplementary Table 3. The resulting raw gene matrices were used as input for downstream analyses using R v3.6.1.

Bioinformatic Processing of scRNA-seq Data

Cell-associated barcodes were determined based on the inflection point of read counts as described previously (Croucher et al. 2021). Low-quality cells were defined as having less than 200 detected genes and/or greater than 20% mitochondrial transcripts and removed from downstream analysis. All subsequent steps in the clustering analysis were performed using Seurat v3.2.1. Briefly, NormalizeData() was used to calculate log-normalized expression values which were inputted to FindVariableGenes() to identify highly variably expressed genes for data scaling using ScaleData(). RunPCA() was then used to compute the top principal components

and the top 10 principal components were used as input for non-linear dimensionality reduction (t-SNE) and graph-based clustering as implemented by Seurat (res=0.6). The plasma cell clusters (C1, C2, C5, C7, n=905 cells) were then subset from the full data set of BM mononuclear cells based on expression of the myeloma marker, *SDC1* (CD138), *TNFRSF17* (BCMA), and *FGFR3,* and re-clustered according to the method described above.

Inferred Copy Number Analysis using sciCNV

The CNV profiles were inferred in pre- (n=340) and post-treatment (n=555) tumor single cells against pooled control NPCs (n=60) using sciCNV method (Mahdipour-Shirayeh et al. 2021) with a sliding-window of 143-gene size and without any baseline correction (see (Mahdipour-Shirayeh et al. 2021) for more details). The input data to sciCNV pipeline was RTAM-normalized (Mahdipour-Shirayeh et al. 2021) in which cells with < 250 expressed genes and genes expressed in < 2% of cells were filtered out. The sciCNV profiles of test and control single cells were, then, scaled at each genomic locus using the mean sciCNV result of test cells to set CNV values to integers. The scaled CNV signals at each locus were denoised against a static noise-threshold of 0.2. Then the sciCNV profile of each cell was standardized against the median of its nearest neighbors to reduce the stochastic noise in the sciCNV output. The final sciCNV results were represented as a heatmap using heatmap.3 R package and by separating pre- and post-treatment tumor cohorts.

Fluorescence In Situ Hybridization (FISH)

Ten thousand CD138+ cells (enriched using magnetic beads, KIT) were centrifuged onto slides with a Shandon Cytospin and fixed in ice-cold 3:1 methanol/acetic acid. Fixed slides were incubated in 2X SSC (pH 7.0) for 10 minutes at 37C, digested with 0.005% pepsin for 10 minutes at 37C, dehydrated in a series of ethanol washes and air-dried. Slides were then denatured in 70% formamide/2X SSC (pH 5.3) for 5 minutes at 72C and hybridized overnight in a humidified chamber with denatured FISH probes. The next day, hybridized slides were washed and mounted in Vectashield/DAPI. Images were acquired on a BioView Allegro fully automated microscope and analyzed with BioView Solo analysis software (BioView USA Inc.). Hybridized slides were then washed, denatured for 3 minutes and re-hybridized with new FISH probes twice to obtain a total of 3 matching sets of images with 7 different FISH probes. Probes used were Vysis LSI IGH/FGFR3

Dual Color Dual FISH probes, Cytocell Aquarius CKS1B/CDKN2C (P18) Amplification/Deletion Probe, Kreatech DLEU1 (13q14)/TP53 (17p13) FISH probe, and Agilent SureFISH 13q34 LAMP1 598kb Aqua probe. At least 300 cells from each slide were scored.

ADDITIONAL INFORMATION

Data Deposition and Access

The novel reported FGFR3 variant has been registered to the ClinGen Allele Registry (Pawliczek et al. 2018) under the Canonical Allele Identifier: CA2573332805. Single-cell data generated from this study is available through the interactive single-cell portal CReSCENT (CRES-P34, https://crescent.cloud/) (Mohanraj et al. 2020).

Ethics Statement

Bone marrow aspirates were obtained with consent under the study protocol approved by the Research Ethics Board at University Health Network, Toronto, Canada (CAPCR #16-5997). The authors declare no competing interests.

Acknowledgements

We gratefully acknowledge the myeloma clinical trials group at Princess Margaret Cancer Centre for their contributions to the FGFR3 clinical trial and coordination of research samples. We thank the staff of the Princess Margaret Genomics Centre (www.pmgenomics.ca, Troy Ketala, Neil Winegarden, Julissa Tsao, Nick Khuu) and Bioinformatics and High-Performance Computing Core (Carl Virtanen, Zhibin Lu, and Natalie Stickle) for sample coordination and their expertise in generating the single-cell sequencing data used in this study.

Author Contributions

DCC, TJP and ST conceived the idea and designed the study. DCC prepared bone marrow samples for sequencing and performed all related data analysis for scRNA-seq. AM performed inferred CNV analysis of the scRNA-seq data using sciCNV. AJD prepared and provided all clinical data for the manuscript. DA provided support for shallow whole genome sequencing analysis. ZL provided support for sample preparation and performed CD138 selection. NE and RT performed cytogenetic FISH analysis. DA, AM, RT, TJP and ST provided guidance in data analysis and interpretation of the results. DCC and AJD drafted the manuscript, with input from TJP and ST. All authors reviewed the manuscript prior to submission.

Funding

The phase 2 clinical trial was supported by Janssen Research and Development and the Multiple Myeloma Research Foundation. Additional research funding was provided by the Princess Margaret Cancer Foundation. Infrastructure support was received from the Canada Foundation for Innovation - John R. Evans Leaders Fund [CFI #38401] and the Ministry of Colleges and Universities Ontario Research Fund - Research Infrastructure Program. DCC was supported by an Ontario Graduate Scholarship, the David Rae Graduate Student Scholarship from the University of Toronto, and a Graduate Fellowship in Cancer Research from the Princess Margaret Hospital Foundation. TJP holds the Canada Research Chair in Translational Genomics and is supported by a Senior Investigator Award from the Ontario Institute for Cancer Research and the Gattuso-Slaight Personalized Cancer Medicine Fund.

REFERENCES

Abdallah N, Rajkumar SV, Greipp P, Kapoor P, Gertz MA, Dispenzieri A, Baughn LB, Lacy MQ, Hayman SR, Buadi FK, et al. 2020. Cytogenetic abnormalities in multiple myeloma: association with disease characteristics and treatment response. *Blood Cancer J* **10**: 82.

Arnulf B, Ghez D, Leblond V, Choquet S, Belhadj K, Macro M, Bouscary D, Facon T, Moreau P, Jaccard A, et al. 2007. FGFR3 Tyrosine Kinase Inhibitor AB1010 as Treatment of t(4;14) Multiple Myeloma. Blood **110**: 413. http://www.bloodjournal.org/content/110/11/413.abstract.

Benard B, Christofferson A, Legendre C, Aldrich J, Nasser S, Yesil J, Auclair D, Liang W, Lonial S, Keats JJ. 2017. FGFR3 Mutations Are an Adverse Prognostic Factor in Patients with t(4;14)(p16;q32) Multiple Myeloma: An Mmrf Commpass Analysis. Blood **130**: 3027. http://www.bloodjournal.org/content/130/Suppl_1/3027.abstract.

Chesi M, Brents LA, Ely SA, Bais C, Robbiani DF, Mesri EA, Kuehl WM, Bergsagel PL. 2001. Activated fibroblast growth factor receptor 3 is an oncogene that contributes to tumor progression in multiple myeloma. Blood **97**: 729–736.

Croucher DC, Richards LM, Tsofack SP, Waller D, Li Z, Wei EN, Huang XF, Chesi M, Bergsagel PL, Sebag M, et al. 2021. Longitudinal single-cell analysis of a myeloma mouse model identifies subclonal molecular programs associated with progression. *Nat Commun* **12**: 6322.

Gibbs L, Legeai-Mallet L. 2007. FGFR3 intracellular mutations induce tyrosine phosphorylation in the Golgi and defective glycosylation. *Biochimica Et Biophysica Acta Bba - Mol Cell Res* **1773**: 502–512.

Huang S, Benavente S, Armstrong EA, Li C, Wheeler DL, Harari PM. 2011. p53 Modulates Acquired Resistance to EGFR Inhibitors and Radiation. *Cancer Res* **71**: 7071–7079.

Kaufman JL, Gasparetto C, Schjesvold FH, Moreau P, Touzeau C, Facon T, Boise LH, Jiang Y, Yang X, Dunbar F, et al. 2021. Targeting BCL-2 with venetoclax and dexamethasone in patients with relapsed/refractory t(11;14) multiple myeloma. *Am J Hematol* **96**: 418–427.

Kumar S, Bianchi G, Biran N, Hultcrantz M, Richter JR, Vij R, Ye JC, Zonder JA, DiLello L, Yesil J, et al. 2022. Myeloma developing regimens using genomics (MyDRUG) trial: Results from the RAS mutation targeting arm. *Journal of Clinical Oncology* **40**: 8055–8055. https://doi.org/10.1200/JCO.2022.40.16_suppl.8055.

Lakshman A, Painuly U, Rajkumar SV, Ketterling RP, Kapoor P, Greipp PT, Dispenzieri A, Gertz MA, Buadi FK, Lacy MQ, et al. 2019. Impact of acquired del(17p) in multiple myeloma. *Blood Adv* **3**: 1930–1938.

Mahdipour-Shirayeh A, Erdmann N, Leung-Hagesteijn C, Tiedemann RE. 2021. sciCNV: high-throughput paired profiling of transcriptomes and DNA copy number variations at single-cell resolution. *Brief Bioinform* **23**.

Masih-Khan E, Trudel S, Heise C, Li Z, Paterson J, Nadeem V, Wei E, Roodman D, Claudio JO, Bergsagel PL, et al. 2006. MIP-1α (CCL3) is a downstream target of FGFR3 and RAS-MAPK signaling in multiple myeloma. Blood **108**: 3465–3471.

Mohanraj S, Díaz-Mejía JJ, Pham MD, Elrick H, Husic M, Rashid S, Luo P, Bal P, Lu K, Patel S, et al. 2020. CReSCENT: CanceR Single Cell ExpressioN Toolkit. Nucleic Acids Res **48**: W372-W379.

Onwuazor ON, Wen X-Y, Wang D-Y, Zhuang L, Masih-Khan E, Claudio J, Barlogie B, Shaughnessy JD, Stewart AK. 2003. Mutation, SNP, and isoform analysis of fibroblast growth factor receptor 3 (FGFR3) in 150 newly diagnosed multiple myeloma patients. Blood **102**: 772–773.

Pawliczek P, Patel RY, Ashmore LR, Jackson AR, Bizon C, Nelson T, Powell B, Freimuth RR, Strande N, Shah N, Paithankar S, Wright MW, Dwight S, Zhen J, Landrum M, McGarvey P, Babb L, Plon SE, Milosavljevic A, on behalf of the Clinical Genome (ClinGen) Resource. 2018. ClinGen Allele Registry links information about genetic variants. Human Mutation **39**: 1690-1701.

Pawlyn C, Davies FE. 2018. Toward personalized treatment in multiple myeloma based on molecular characteristics. Blood **133**: 660–675.

Plowright EE, Li Z, Bergsagel PL, Chesi M, Barber DL, Branch DR, Hawley RG, Stewart AK. 2000. Ectopic expression of fibroblast growth factor receptor 3 promotes myeloma cell proliferation and prevents apoptosis. Blood **95**: 992–8.

Ronchetti D, Greco A, Compasso S, Colombo G, Dell'Era P, Otsuki T, Lombardi L, Neri A. 2001. Deregulated FGFR3 mutants in multiple myeloma cell lines with t(4;14): comparative analysis of Y373C, K650E and the novel G384D mutations. *Oncogene* **20**: 3553–3562.

Rousseau F, Saugier P, Merrer ML, Munnich A, Delezoide A-L, Maroteaux P, Bonaventure J, Narcy F, Sanak M. 1995. Stop codon FGFR3 mutations in thanatophoric dwarfism type 1. *Nat*

Genet **10**: 11–12.

Scheid C, Reece D, Beksac M, Spencer A, Callander N, Sonneveld P, Kalimi G, Cai C, Shi M, Scott JW, et al. 2015. Phase 2 study of dovitinib in patients with relapsed or refractory multiple myeloma with or without t(4;14) translocation. *Eur J Haematol* **95**: 316–324.

Trudel S, Bergsagel PL, Singhal S, Niesvizky R, Comenzo RL, Bensinger WI, Lebovic D, Choi Y, Lu D, French D, et al. 2012. A Phase I Study of the Safety and Pharmacokinetics of Escalating Doses of MFGR1877S, a Fibroblast Growth Factor Receptor 3 (FGFR3) Antibody, in Patients with Relapsed or Refractory t(4;14)-Positive Multiple Myeloma. Blood **120**: 4029. http://www.bloodjournal.org/content/120/21/4029.abstract.

Trudel S, Ely S, Farooqi Y, Affer M, Robbiani DF, Chesi M, Bergsagel PL. 2004. Inhibition of fibroblast growth factor receptor 3 induces differentiation and apoptosis in t(4;14) myeloma. Blood **103**: 3521–3528.

Wesche J, Haglund K, Haugsten EM. 2011. Fibroblast growth factors and their receptors in cancer. *Biochem J* **437**: 199–213.

Zheng GXY, Terry JM, Belgrader P, Ryvkin P, Bent ZW, Wilson R, Ziraldo SB, Wheeler TD, McDermott GP, Zhu J, et al. 2017. Massively parallel digital transcriptional profiling of single cells. *Nature Communications* **8**: 1–12.

FIGURES

Figure 1. Delineation of transcriptional heterogeneity in myeloma cells before and after treatment with erdafitinib. (A) tSNE visualization of 965 myeloma cells from erdafitinib pre-treatment and C2D1 samples, coloured by cluster identity or sample identity **(B)**. **(C)** Distribution of myeloma cells profiled by scRNA-seq across transcriptional clusters for pre-treatment and C2D1 samples. **(D)** Heatmap depicting top 20 marker genes upregulated in each myeloma transcriptional cluster as determined by differential expression analysis ($P<0.05$). A subset of 75 randomly selected cells per transcriptional cluster is shown and data represents scaled expression values (any values outside a range of -2 to 2 were clipped).

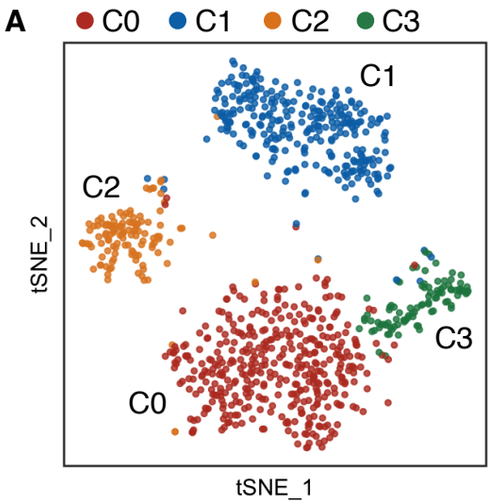
A
C0
C1
C2
C3
C1
C2
C3
C0
tSNE_2
tSNE_1

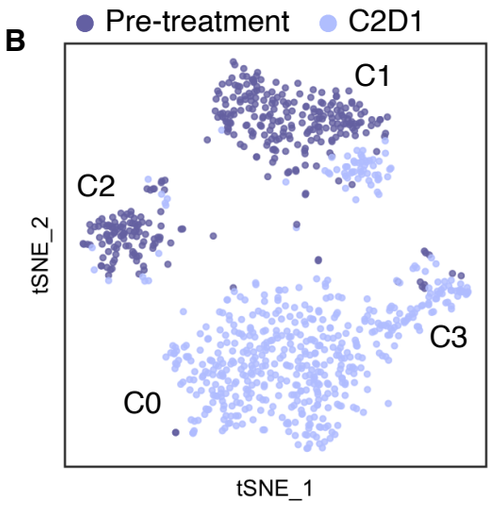
B
Pre-treatment
C2D1
C1
C2
C3
C0
tSNE_2
tSNE_1

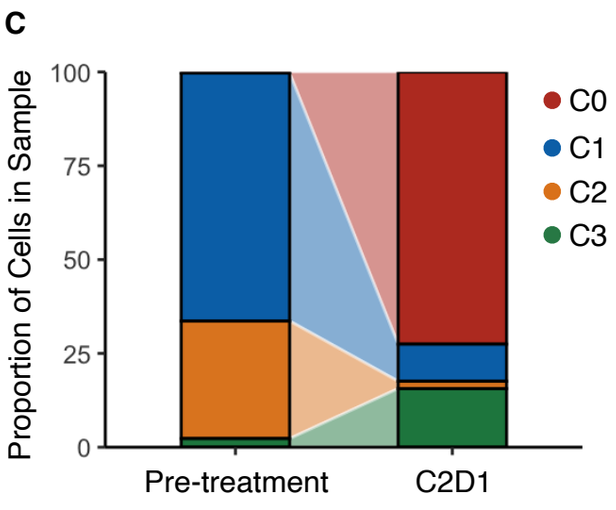
C
Proportion of Cells in Sample
100
75
50
25
0
C0
C1
C2
C3
Pre-treatment
C2D1

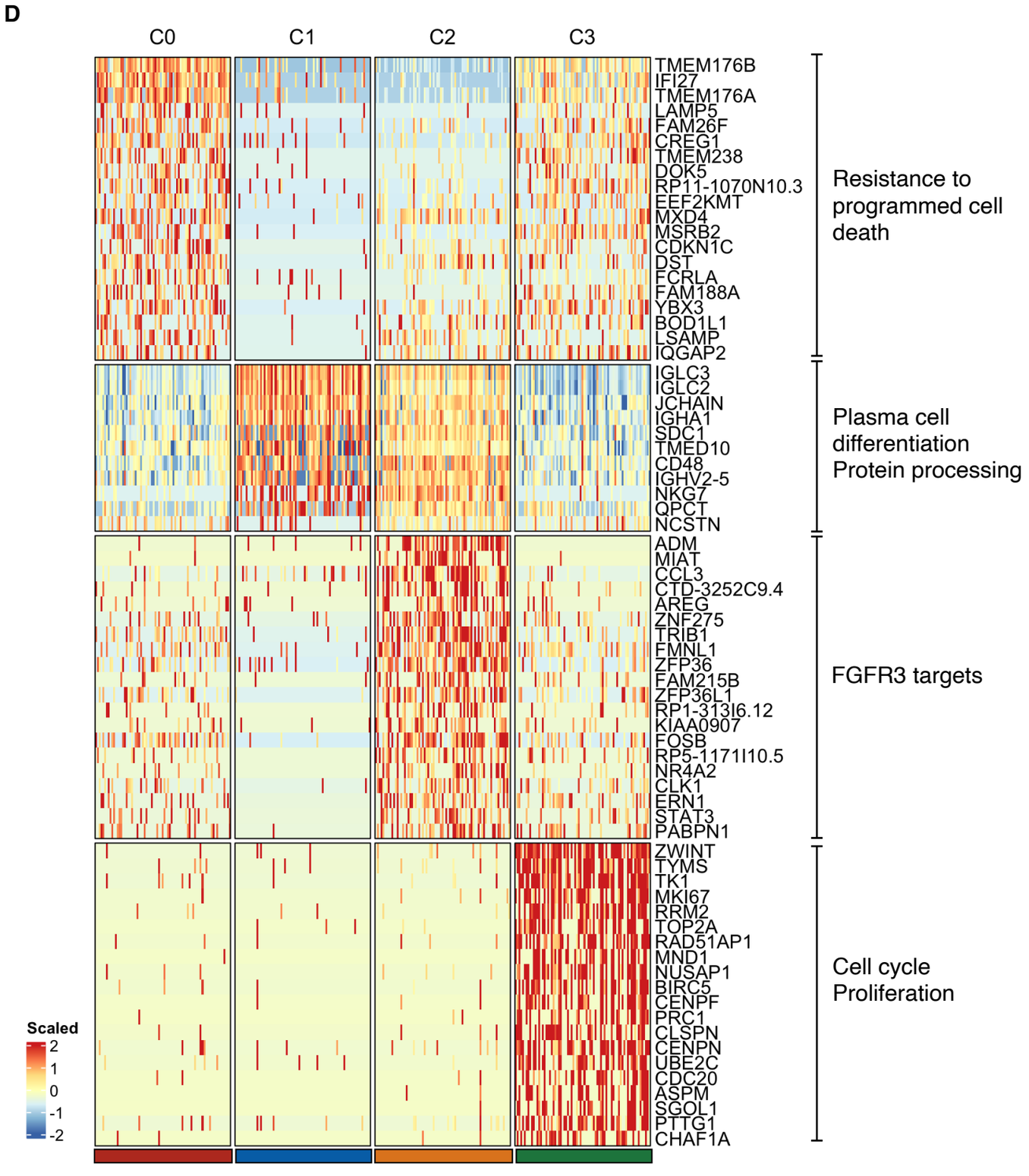
D
C0
C1
C2
C3
TMEM176B
IFI27
TMEM176A
LAMP5
FAM26F
CREG1
TMEM238
DOK5
RP11-1070N10.3
EEF2KMT
MXD4
MSRB2
CDKN1C
DST
FCRLA
FAM188A
YBX3
BOD1L1
LSAMP
IQGAP2
IGLC3
IGLC2
JCHAIN
IGHA1
SDC1
TMED10
CD48
IGHV2-5
NKG7
QPCT
NCSTN
ADM
MIAT
CCL3
CTD-3252C9.4
AREG
ZNF275
TRIB1
FMNL1
ZFP36
FAM215B
ZFP36L1
RP1-313I6.12
KIAA0907
FOSB
RP5-1171I10.5
NR4A2
CLK1
ERN1
STAT3
PABPN1
ZWINT
TYMS
TK1
MKI67
RRM2
TOP2A
RAD51AP1
MND1
NUSAP1
BIRC5
CENPF
PRC1
CLSPN
CENPN
UBE2C
CDC20
ASPM
SGOL1
PTTG1
CHAF1A
Resistance to programmed cell death
Plasma cell differentiation Protein processing
FGFR3 targets
Cell cycle Proliferation
Scaled
2
1
0
-1
-2

Figure 2. Subclonal copy number alternations inferred from individual myeloma cells. (A) Heatmap of genome-wide copy number variation inferred from scRNA-seq data of malignant plasma cells as determined using sciCNV (Mahdipour-Shirayeh et al. 2021) using normal plasma cells (NPC) from BMMC as reference. Columns represent genome position across chromosomes. **(B)** Gene set scoring for chromosome 17p module score (MSigDB Positional Geneset) calculated using Seurat's AddModuleScore in malignant cells across treatment groups. Boxplots represent the distribution of each measurement within treatment groups, where the central rectangle spans the interquartile range and then the central line represents the median, and "whiskers" above and below the box show the value 1.5x the IQR. Cells from the pre-treatment sample scoring less than 1.5x below the IQR are highlighted red (outlier) and inferred to be 17p deleted subclones. **(C)** Fluorescence microscopy images of representation cells from top three cytogenetic subclones. Probes are colour-coded above each image with corresponding karyotypes below. Counted cells are listed to the right of each subclone expressed relative to the total t(4;14) malignant cells counted. **(D)** Hypothetical evolutionary path of CNV subclones based on karyotypes from FISH analysis. Subclonal proportions are listed to the right of each subclone expressed relative to total cells counted (normal and malignant).

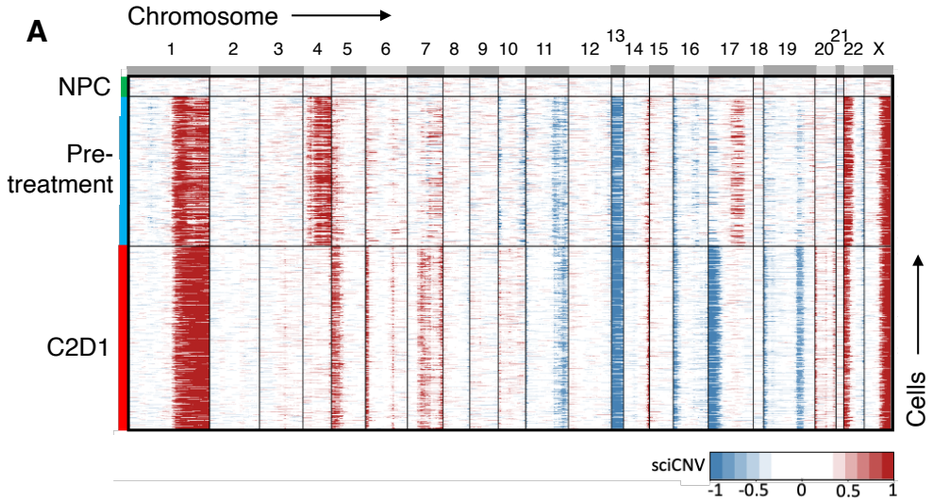
A
Chromosome
1 2 3 4 5 6 7 8 9 10 11 12 13 14 15 16 17 18 19 20 21 22 X
NPC
Pre-treatment
C2D1
Cells
sciCNV
-1 -0.5 0 0.5 1

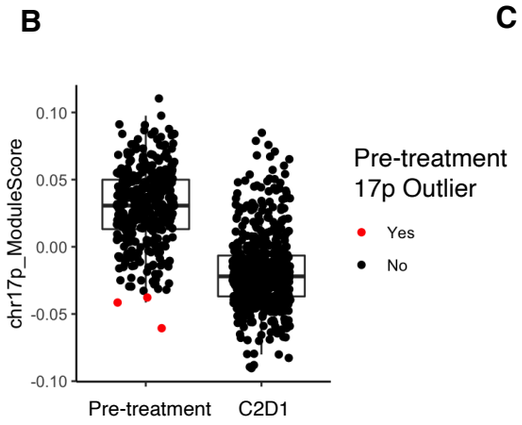
B
chr17p_ModuleScore
0.10
0.05
0.00
-0.05
-0.10
Pre-treatment
C2D1
Pre-treatment 17p Outlier
Yes
No

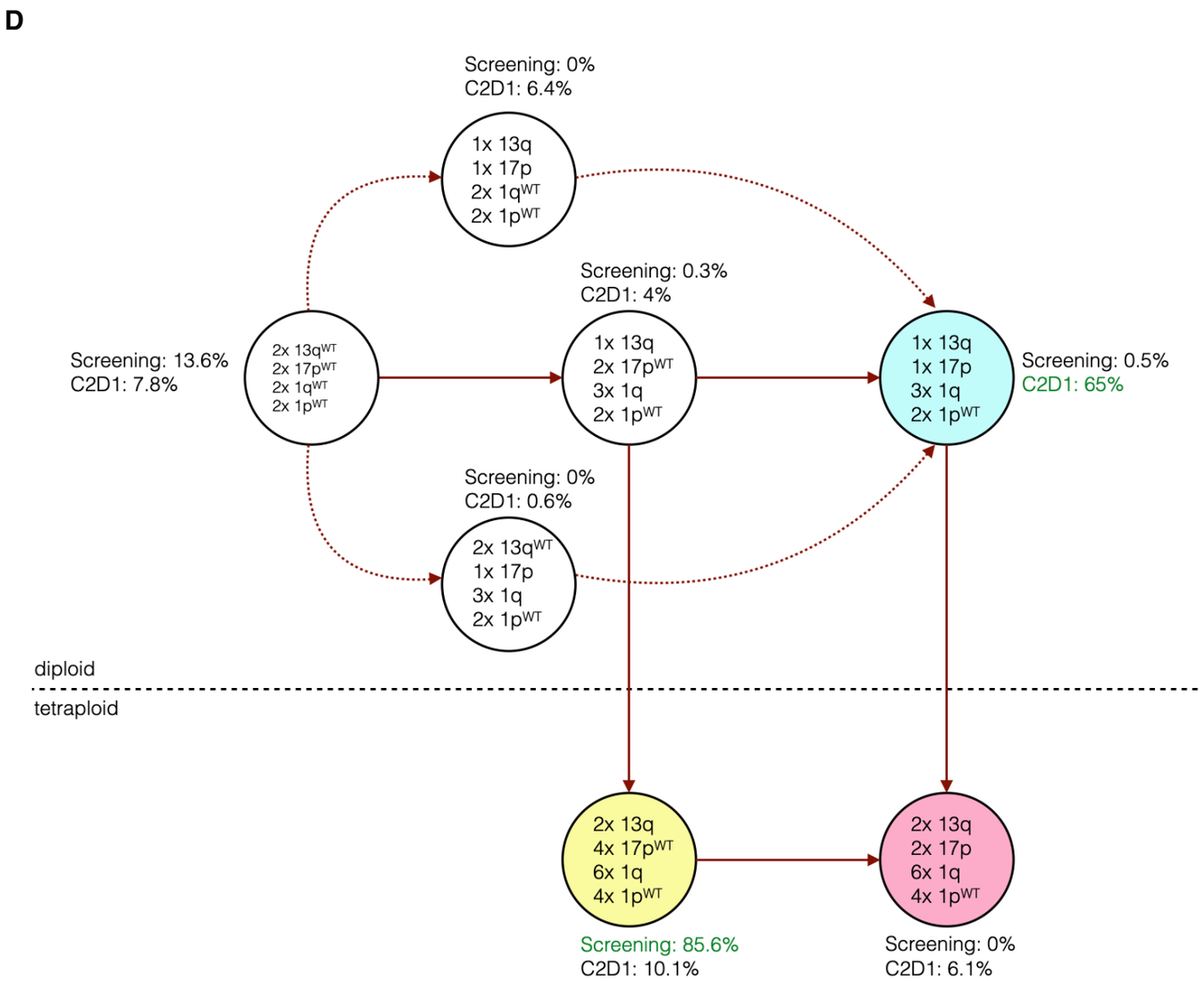
D
Screening: 0%
C2D1: 6.4%
1x 13q
1x 17p
2x 1q^WT
2x 1p^WT
Screening: 0.3%
C2D1: 4%
Screening: 13.6%
C2D1: 7.8%
2x 13q^WT
2x 17p^WT
2x 1q^WT
2x 1p^WT
1x 13q
2x 17p^WT
3x 1q
2x 1p^WT
1x 13q
1x 17p
3x 1q
2x 1p^WT
Screening: 0.5%
C2D1: 65%
Screening: 0%
C2D1: 0.6%
2x 13q^WT
1x 17p
3x 1q
2x 1p^WT
diploid
tetraploid
2x 13q
4x 17p^WT
6x 1q
4x 1p^WT
Screening: 85.6%
C2D1: 10.1%
2x 13q
2x 17p
6x 1q
4x 1p^WT
Screening: 0%
C2D1: 6.1%

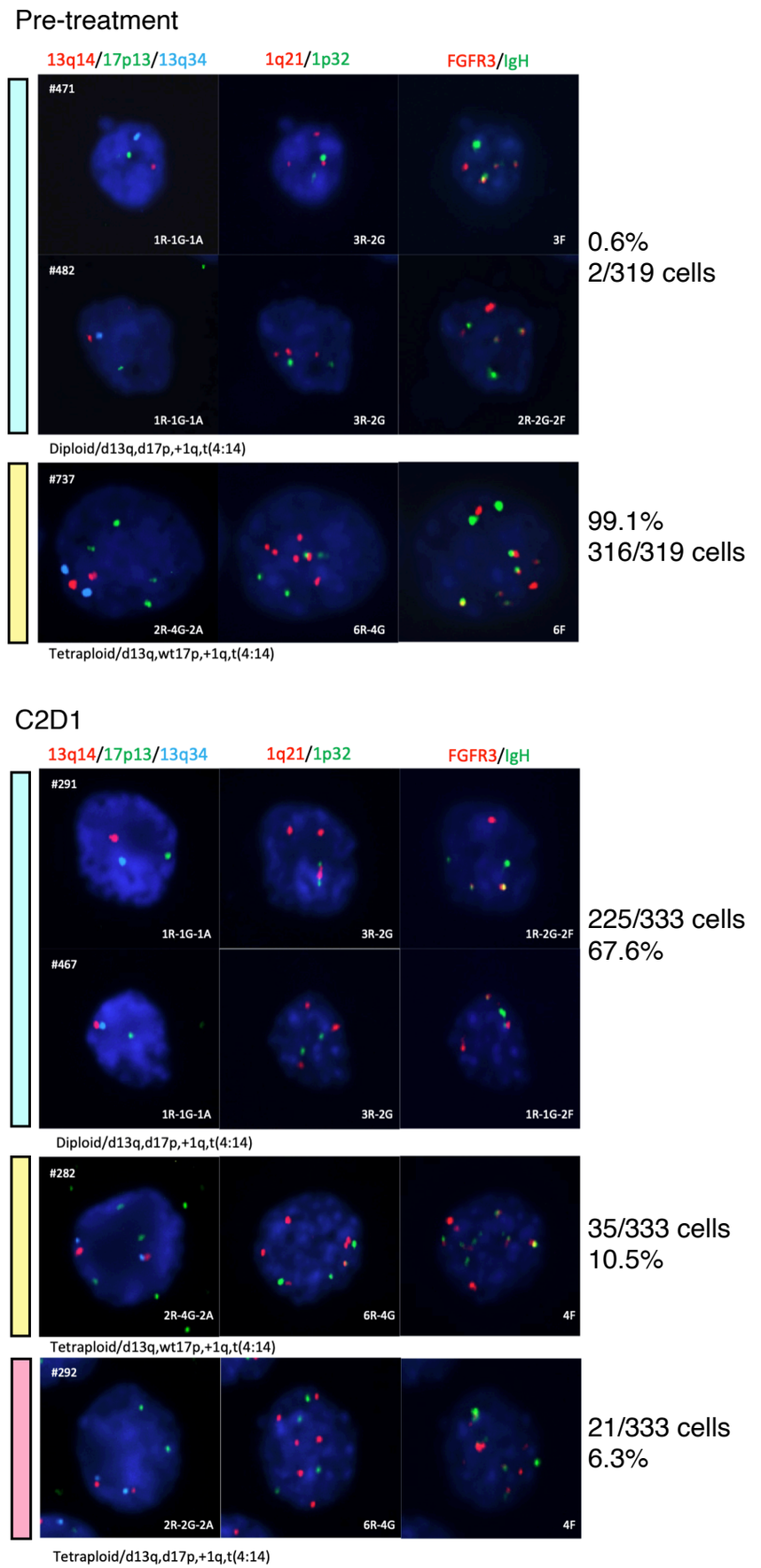
C
Pre-treatment
13q14/17p13/13q34
1q21/1p32
FGFR3/IgH
#471
1R-1G-1A
3R-2G
3F
#482
1R-1G-1A
3R-2G
2R-2G-2F
Diploid/d13q,d17p,+1q,t(4:14)
0.6%
2/319 cells
#737
2R-4G-2A
6R-4G
6F
Tetraploid/d13q,wt17p,+1q,t(4:14)
99.1%
316/319 cells
C2D1
13q14/17p13/13q34
1q21/1p32
FGFR3/IgH
#291
1R-1G-1A
3R-2G
1R-2G-2F
#467
1R-1G-1A
3R-2G
1R-1G-2F
Diploid/d13q,d17p,+1q,t(4:14)
225/333 cells
67.6%
#282
2R-4G-2A
6R-4G
4F
Tetraploid/d13q,wt17p,+1q,t(4:14)
35/333 cells
10.5%
#292
2R-2G-2A
6R-4G
4F
Tetraploid/d13q,d17p,+1q,t(4:14)
21/333 cells
6.3%

Figure 3. Identification of FGFR3 stop-loss deletion in scRNA-seq reads from pre-erdafitinib treated myeloma cells. (A) IGV screenshot of FGFR3 gene loci on chromosome 4 depicting reads from scRNA-seq that contain the p.G802_X807del stop-loss loss deletion (grouped by cell barcode). **(B)** tSNE visualization of 965 myeloma cells from erdafitinib pre-treatment and C2D1 samples with cells containing the p.G802_X807del stop-loss deletion coloured according to corresponding cell barcode colours from Figure 3A or grey if no reads coverage at the p.G802_X807del stop-loss deletion loci. **(C)** Proposed model for molecular response to erdafitinib as determined by scRNA-seq profiling.

A

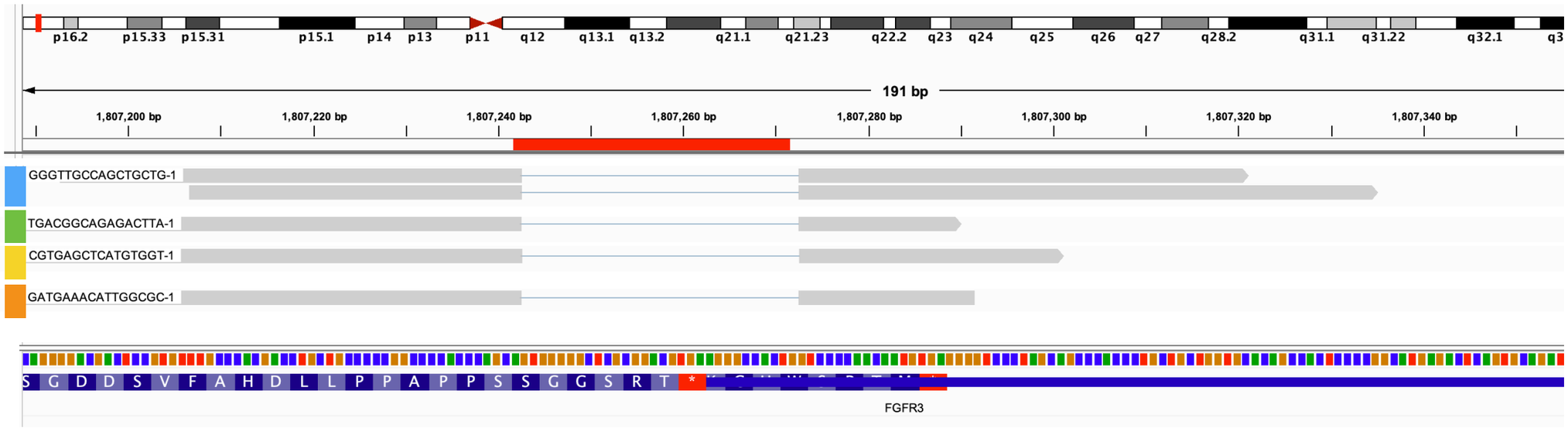
p16.2
p15.33
p15.31
p15.1
p14
p13
p11
q12
q13.1
q13.2
q21.1
q21.23
q22.2
q23
q24
q25
q26
q27
q28.2
q31.1
q31.22
q32.1
q3
191 bp
1,807,200 bp
1,807,220 bp
1,807,240 bp
1,807,260 bp
1,807,280 bp
1,807,300 bp
1,807,320 bp
1,807,340 bp
GGGTTGCCAGCTGCTG-1
TGACGGCAGAGACTTA-1
CGTGAGCTCATGTGGT-1
GATGAAACATTGGCGC-1
S G D D S V F A H D L L P P A P P S S G G S R T *
FGFR3

B

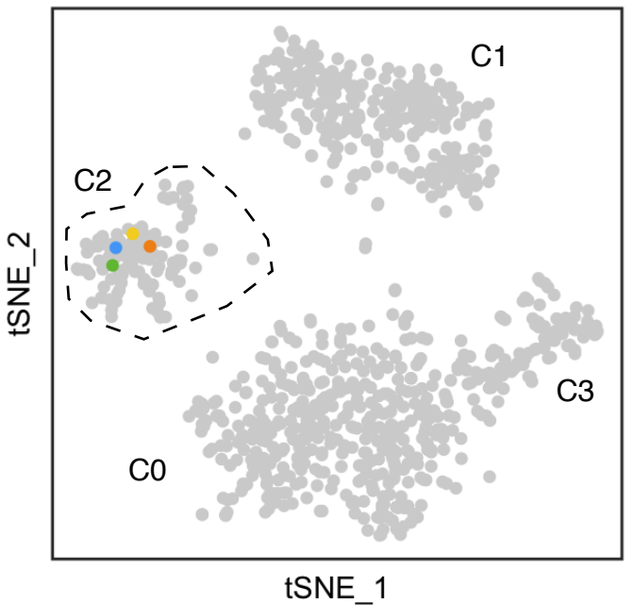
C1
C2
C3
C0
tSNE_2
tSNE_1

C

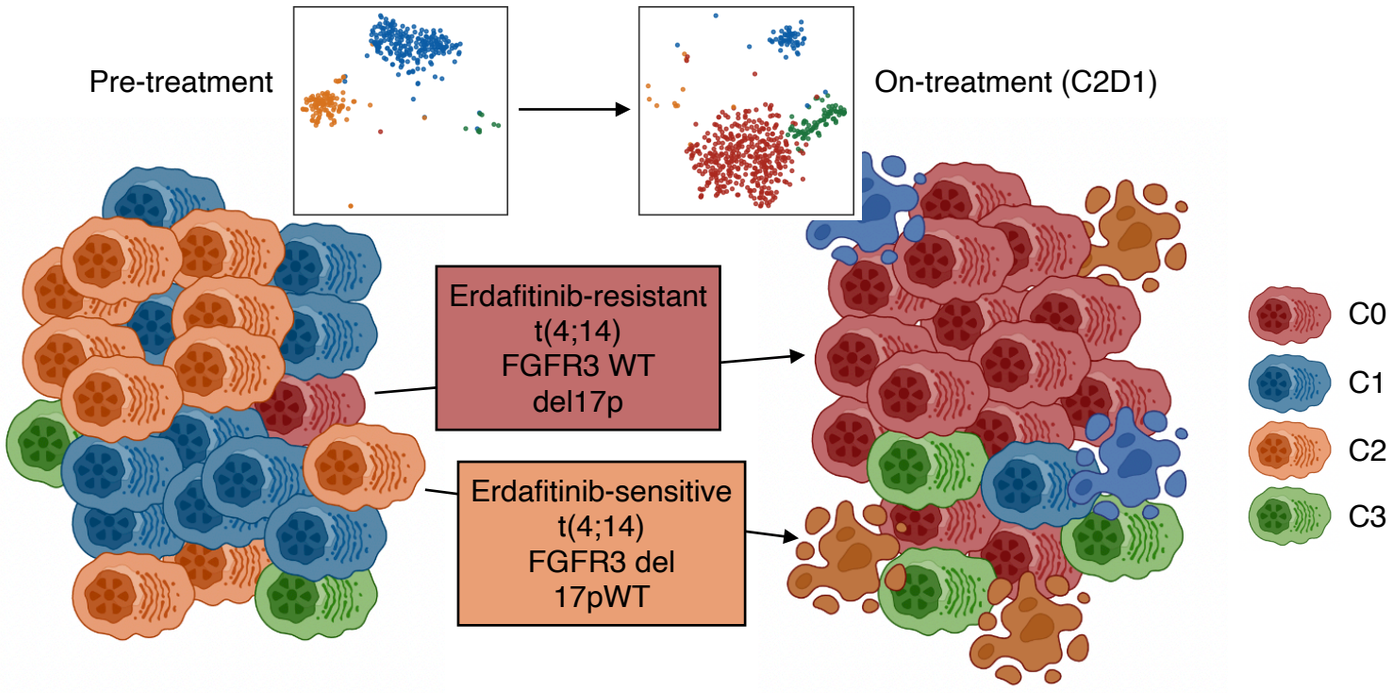
Pre-treatment
On-treatment (C2D1)
Erdafitinib-resistant
t(4;14)
FGFR3 WT
del17p
Erdafitinib-sensitive
t(4;14)
FGFR3 del
17pWT
C0
C1
C2
C3

Gene	Chromosome	HGVS DNA Reference	HGVS Protein Reference	Variant Type	Predicted Effect (substitution, deletion, etc.)	dbSNP/ dbVar ID	Genotype (heterozygous/ homozygous)
FGFR3	Chr4:1808969	c.2404_*12delGGGGGCTCGCGGACGTGAAGGGCCACTGGT	p.Gly802_Ter807del	In-frame deletion	Stop-loss	N/A	Somatic (AF=19%)
EED	Chr11:85977170	c.772C>A	p.His258Asn	Missense	Substitution	N/A	Somatic (AF=10%)
LRP1B	Chr2:141680558	c.3295A>G	p.Thr1099Ala	Missense	Substitution	N/A	Somatic (AF=15%)
MYC	Chr8:128753085	c.1246G>T	p.Ala416Ser	Missense	Substitution	N/A	Somatic (AF=20%)
BCOR	ChrX:39934048	c.551C>T	p.Ala184Val	Missense	Substitution	N/A	Somatic (AF=19%)

Table 1. Summary of variants detected by the OncoSeq 1500 assay as part of the MMRF MI-ONCOSEQ clinical sequencing study (NCT0288410).

Single-cell profiling of multiple myeloma reveals molecular response to FGFR3 inhibitor despite clinical progression

Danielle C Croucher, Anup Joseph Devasia, Dor D Abelman, et al.

Cold Spring Harb Mol Case Stud published online January 13, 2023
Access the most recent version at doi:10.1101/mcs.a006249